REPORT DOCUMENTATION PAGE

Form Approved
OMB No. 0704-0188

1. AGENCY USE ONLY (Leave blank)
2. REPORT DATE: 1995
3. REPORT TYPE AND DATES COVERED: Interim

4. TITLE AND SUBTITLE
Ground State Characteristics and Optical Spectra of Ce and Eu Octaethyl Bisporphyrinate Double Deckers

5. FUNDING NUMBERS
N00014-90-J-1608
G

6. AUTHOR(S)
Guillermina L. Estiu, Notker Roesch and Michael C. Zerner

7. PERFORMING ORGANIZATION NAME(S) AND ADDRESS(ES)
University of Florida
Department of Chemistry
Gainesville, FL 32611 USA

8. PERFORMING ORGANIZATION REPORT NUMBER

9. SPONSORING/MONITORING AGENCY NAME(S) AND ADDRESS(ES)
Office of Naval Research
Chemistry Division Code 1113
Arlington, VA 22217-5000

10. SPONSORING/MONITORING AGENCY REPORT NUMBER
Technical Report 34

11. SUPPLEMENTARY NOTES
To be submitted for publication.

12a. DISTRIBUTION/AVAILABILITY STATEMENT
This document has been approved for public release: its distribution is unlimited.

12b. DISTRIBUTION CODE

13. ABSTRACT (Maximum 200 words)

See attached Abstract.

14. SUBJECT TERMS

15. NUMBER OF PAGES
44

16. PRICE CODE

17. SECURITY CLASSIFICATION OF REPORT	18. SECURITY CLASSIFICATION OF THIS PAGE	19. SECURITY CLASSIFICATION OF ABSTRACT	20. LIMITATION OF ABSTRACT
Unclassified	Unclassified	Unclassified	SAR

19950705 041

Per Anne Watson at Office of Naval research Arlington Va (DSN: 226-4108) they sent what they have and unable to get the missing pages.

October 2, 1995

OFFICE OF NAVAL RESEARCH

GRANT or CONTRACT N00014-90-J-1608

R&T CODE 4131057- - - 01

Technical Report No. 34

Ground State Characteristics and Optical Spectra of Ce and Eu Octaethyl Bisporphyrinate Double Deckers

by

Guillermina L. Estiú, Notker Rösch and Michael C. Zerner

To be Submitted for Publication

University of Florida
Department of Chemistry
Quantum Theory Project
Gainesville, FL 32611-8435

April 18, 1995

Ground State Characteristics and Optical Spectra of Ce and Eu Octaethyl Bisporphyrinate Double Deckers

Guillermina L. Estiú [1], Notker Rösch [2], and Michael C. Zerner [3]

1- Programa Quinor, Departamento de Quimica, Fac. Cs. Exactas, UNLP-Casilla de Correo 962, 1900-La Plata y Departamento de Ciencia y Tecnologia, Univ. Nac. de Quilmes, Roque Saenz Peña 180, 1876-Bernal, Argentina.

2- Technische Universität München, D-85747 Garching, Germany.

3- Quantum Theory Project, University of Florida, Gainesville, FL 32611, USA.

ABSTRACT

The ground state electronic structure and optical spectra of Ce(III), Ce(IV) and Eu(III) octaethyl bisporphyrin dimers (double deckers) are examined using the Intermediate Neglect of Differential Overlap (INDO/S) model and multireference configuration interaction (MRCI). The low energy electronic exited states of the dimers are interpreted in terms of their monomer contributions, and the charge transfer and excitonic character of the transitions are analyzed. Particular attention is focused on the nature of the near infrared band (NIR) that characterizes the spectra of the electron deficient bisporphyrin dimers, justifying its shift to higher energy as the ionic radii of the central ion decreases, and relating its broadness to the contribution of closely spaced electronic transitions that become allowed through vibronic coupling. The influence of an electric perturbation on the dimeric Ce(IV) and Eu(III) structures is used to explain their conductivity. The results are compared to those derived from resonant Raman spectroscopy, which show the importance of the vibrational fine structure in the assignment of the NIR band.

1. INTRODUCTION

Lanthanide porphyrin double deckers, $Ln(P)_2$,[1] are intensively studied as prospective materials for electrical devices.[2-6] The closely spaced porphyrin π systems allow strong electronic interactions between the units, and impart unique electron transfer and/or conductivity properties to the system. The distance between the tetrapyrrole ligands plays an important role because the electronic interactions may involve π overlap between the macrocycles, which can be adjusted by means of a proper selection of the central atom.[7] It has been claimed that, for these kinds of compounds, as well as for those in which the central atom is either an actinide or a transition metal, the charge transfer interaction resembles that of the bacterial photosynthetic reaction,[3,7-9] in which two bacterioclorophyl molecules, closely associated, constitute the *special pair*, a supermolecule that serves as the primary electron donor in light energy conversion.[10,11] The lanthanide double deckers have been used to mimic the interactions within the dimer of the photosynthetic reaction center. They show analogies to the special pair in that both are easily oxidized and that both have a low energy first (π, π^*) excited state in comparison to the monomeric chromophores.[3] Exciton (dipole-dipole) (Ex) coupling of the lowest states of the subunits, together with charge transfer (CT) configurations, have been used to explain the origin of the electronic properties of the special pair.[7,12-15] Both effects depend on the degree of interaction between the subunits. Strongly interacting systems are usually better analyzed, on the other hand, in a supermolecule approach, as the definition of the molecular orbitals strictly localized on each subunit becomes questionable.

In order to study the influence of the separation of the π systems on the electronic characteristics, and the relative importance of the different effects (Ex, CT) as a function of this separation, not only lanthanide (Ln), but also actinide (Ac) and transition metal (TM) bisporphyrin sandwich complexes have been investigated. In these studies the mean separation between the nitrogen planes of the two porphyrin subunits varies from 2.9 Å (Ac)[7,16] to 2.8

April 5, 1995

Å (Ln)[2-6] and 2.6 Å (TM).[17-19] These sandwich complexes show optical characteristics that are not exhibited by porphyrin dimers having larger separations between the macrocycles. In the former case there is a broad absorption 1,000–3,000 cm^{-1} to the red of the Q absorption of monoporphyrins and a prominent near infrared (NIR) feature appears in the spectra of complexes with an odd electron number or in (π, π^*) excited states.[2-7] Distortions from planarity also seem to play a role, and the effect of non-planar conformations, often resulting from steric crowding of peripheral substituents attached to the methine or β carbons, in modifying the properties of tetrapyrrols, have been an active area of investigation.[20,21] Octaethyl and tetraphenyl bisporphyrins (OEP, TTP) are considered as model compounds for the investigation of the relationship between non-planarity and a particular function, such as the capacity of the system to accept or donate an electron in electron transfer systems. Another important variation of the sandwich system may be obtained by changing the central atom, which, in turn, influences the distance between the π moieties. In the Ln series, a decrease in the energy of the NIR band parallels the increase in the ionic radius of the central metal ion and, thus, the ring-ring distances in the double decker, a fact that is likely to be associated to some steric effect, without involvement of the f electrons.[9]

Much speculation has surrounded the origin of the NIR band. The origin of this transition was first assigned to an internal (intervalence) charge transfer transition between one neutral and one fully oxidized porphyrin moiety.[2] The position of the band on the energy scale was then used to quantify the charge transfer capability of a given dimeric complex. Later studies, based on UV-visible absorption and resonance Raman (RR) spectroscopy, indicate that the hole is delocalized over the π system of the two monomers in both the vibrational (10^{-13} s) and electronic (10^{-15} s) time scales.[6] The π overlap between the two units is distance dependent, and is strongly affected by the size of the central atom and by distortions from planarity. Moreover, RR spectroscopy indicates that the hole is located in a porphyrin a_{1u} derived dimer molecular orbital (MO) and,

on this basis, it has been inferred that the NIR absorption band might be associated with the promotion of an electron from a filled b_1 (bonding) to a half-filled a_2 (antibonding) MO in D_{4d} symmetry, a z-polarized allowed transition whose energy is determined, in part, by the extent of the interaction between the ring systems.[6]

In this paper quantum chemical calculations are used to study these systems. We seek an explanation for the origin of the NIR transition and the different effects associated with it. We focus this work on two bisporphyrin lanthanide complexes whose structure and spectroscopic characteristics are well established[2,5] and thus allow an appropriate evaluation of the results. We have chosen, to this end, Eu and Ce bisoctaethylporphyrinates, comparing the spectra of the former to those of the neutral and oxidized species of the latter. The neutral $Ce(OEP)_2$ complex is the only case where the NIR band does not develop. All other lanthanide complexes, containing Ln(III) ions, give porphyrin π radicals characterized by NIR absorption bands whose position in the energy scale correlates inversely with the ionic radii on the central ion. However, diamagnetic $Ce(OEP)_2$ is easily oxidized to the radical cation $[Ce(OEP)_2]^+$, which also displays the characteristic NIR absorption at 1270 nm. In addition to the assignment of the UV-visible spectra, we discuss the electronic characteristics of the ground state of the lanthanide complexes, mainly focusing on the oxidation state of the central atom.

2. THEORETICAL METHODS

We examine these systems using the Intermediate Neglect of Differential Overlap (INDO) model[22-24] parameterized for spectroscopy (INDO/S)[25–28] at the Configuration Interaction Singles (CIS) level of theory,[25–28] and that has been recently successfully extended to the lanthanide series.[29–31]

All self consistent field (SCF) calculations were of the Restricted Hartree Fock type, defining either close or open shell operators (RHF, ROHF) for the $Ce(OEP)_2$, $[CE(OEP)_2]^+$, and $Eu(OEP)_2$

complexes. In the latter, Configuration Average HF[32,33] has been used to average 9 electrons of the Eu atom assigned to the 7 f orbitals. The SCF calculations were followed by a configuration interaction (CI) treatment, using a Rumer diagram technique[34,35] for the open-shell structures. A total of 350, 360, and 1044 configurations were included for the $Ce(OEP)_2$, $[Ce(OEP)_2]^+$, and $Eu(OEP)_2$ calculations, respectively, 14 orbitals down and 10 up for the Ce complexes and 15 down and 14 up for the Eu compound. The CI calculations were performed under C_{2v} symmetry. Spin-orbit interaction was not taken into account. The results are reported under D_{4d} symmetry, which is the actual symmetry of the idealized sandwich structures, Figure 1. Oscillator strengths are evaluated with the dipole-length operator[36,37] retaining all one-center terms. In general, the model reproduces the energy of the Q bands of porphyrins and hydroporphyrins very well, but overestimates the higher energy B bands by about 5,000 cm^{-1}, see later.

The geometry of the $Ln(OEP)_2$ complexes was taken from X-ray crystallographic data.[2,5] The central ion is surrounded by eight nitrogen atoms of the two porphyrin rings, and its coordination polyhedron is nearly a square antiprism, with the porphyrin rings rotated by an angle close to 45 degrees from the eclipsed position (Fig. 1a). The four pyrrole N atoms (N_p) on each of the macrocycles are coplanar within experimental error, and separated by 2.752 and 2.848 Å in the Ce and Eu complexes, respectively. Both macrocycles are convexed and severely distorted from planarity (Fig. 1.b). This deformation improves the overlap of the donor pairs of the eight N_p atoms with the large central metal acceptor ion which is too large to sit in the center of a single porphyrinate ligand. The doming decreases as the ionic radius of the Ln ion increases, defining dihedral angles between the pyrrol planes and the planes of the four N_p atoms, with an average value of 12.2 and 15.5 degrees for the Eu and Ce complexes, respectively. These structural characteristics have been considered in the calculations, although the ethyl substituents on each pyrrole ring were not explicitly included.

$Ce(OEP)_2$, $[CE(OEP)_2]^+$, and $Eu(OEP)_2$ have been calculated using an idealized D_{4d} sym-

metry. The actual structure involves distortions from this symmetry which might affect the intensity of the calculated spectroscopic features.

3. RESULTS AND DISCUSSION

3.1 $Ce(OEP)_2$, neutral and cationic species

3.1a Ground state calculations Neutral $Ce(OEP)_2$ is known to be diamagnetic,[2] and an oxidation state +IV on the central atom is generally accepted[4,6]. Our SCF/CI calculations show that the ground state (GS) is $^1A_1$ in D_{4d} symmetry, which is 0.996 and 1.091 eV more stable than the two lowest triplets, of $^3E_3$ and $^3E_1$ symmetry, respectively. The next singlet, $^1E_3$, is calculated to lie 1.688 eV above the GS, followed by two triplets, $^3E_1$ and $^3E_3$, that are only 0.065 and 0.100 eV higher in energy.

A Mulliken population analysis gives a positive charge of +0.37 au to the central atom, with essentially no population in the f orbitals. The $4f^{0.12}6s^{0.41}6p^{0.89}5d^{2.21}$ electronic configuration is interpreted through an electronic back donation from the porphyrin rings to the s, p, d, and f metal orbitals. There is no formal d orbital occupation. The small occupation of the f orbitals can be related to minor contributions of a Ce(III) oxidation state, but Ce(IV) clearly dominates the GS description. An intermediate oxidation state would imply an equilibrium between $Ce^{+4}[(OEP)^{-2}]_2$ and $Ce^{+3}[(OEP)_2]^{-3}$ species. While the first formula involves two typical porphyrinate dianions, the latter may be represented as a Ce^{+3} ion associated either with one normal porphyrinate dianion and one monoanion radical, $[Ce^{+3}(OEP)^{-2}\ (OEP)^{-}]$, or with two porphyrin with delocalized orbitals with net charge -3. According to our calculations the former, non-symmetrical structure, where the unpaired electron is localized on one of the rings, can be ruled out on the basis of identical electronic populations on both porphyrin moieties, even after modest geometric distortion. We find the unpaired electron delocalized over the two porphyrin rings, and the spin is cancelled with that of the central metal to give anti-ferromagnetic

exist between each OEP and the Ce(IV) atom, just like in cyclopentadianyl sandwich compounds of transition metals) and a small 0.19 bond index directly between the two OEPs. The interactions between the three fragments remain strong even when the interring distance is increased to 4.0 Å: the metal-ring bond index decreases only to 2.72 and the bond index between the two OEPs to 0.07.

Electrochemical oxidation generates the π cation radical $Ce[(OEP)_2]^+$. The ease of oxidation suggests that the redox orbital is delocalized over both porphyrin π systems,[4] and agrees, in this way, with the equivalent electronic populations on both rings that results from our calculations. According to our multi-reference CI (MRCI) calculations, the GS of the paramagnetic $Ce[(OEP)_2]^+$ is $^2A_2$ with an unpaired electron in the HOMO a_2, followed by $^2B_1$, $^2B_2$ and $^2A_1$ states that are calculated 0.988, 1.072, and 1.157 eV, respectively, higher in energy, and that are associated with the promotion of an electron from the b_1, b_2, and a_1 orbitals to the a_2 orbital that is singly occupied in the GS of the cation. At higher energies lie $^2E_3$ and $^2E_1$ states that result from the promotion of the unpaired electron in the HOMO a_2 to the degenerate LUMO orbitals and these are calculated to be 1.186 and 1.381 eV higher in energy than the GS. In turn, $^4E_3$ and $^4E_1$ states are calculated at 1.568 and 1.762 above the $^2A_2$ ground state.

A Mulliken population analysis of the cation does not show any change of the oxidation state on the central atom (consistent with our Ce (IV) interpretation), which bears the same local charge (+0.34 au) as does the neutral species, with a $4f^{0.15}6s^{0.41}6p^{0.86}5d^{2.24}$ electronic configuration. The change in the population is clearly localized on the porphyrin rings.

The lowest energy $^2A_2$ state as described above is formed by removing an electron from the a_2 orbital (Fig. 2). The same conclusion results from spectroscopic studies on the cationic species, as well as on complexes that are isoelectronic with it, and are also characterized by a hole in the electronic π system. In particular, RR spectroscopy indicates that the hole resides in a $a_{1u}(\pi)$ derived MO of the porphyrin ring.[6]

3.1b UV-visible spectroscopy The double decker $Ce(OEP)_2$ exhibits some features that are characteristic of a lanthanide porphyrin.[2,39] There are strong bands with the appearance of B(Soret), Q_1 and Q_0 bands at 26,455; 18,870, and 17,452 cm^{-1}, respectively (Fig. 3). The Soret also shows a shoulder 3,000 cm^{-1} to the blue (Fig. 3).[2,4] The Soret band is, however, hypsocromically shifted (higher energy) compared to a lanthanide monoporphyrin, a fact that has been attributed to exitonic interactions between the B excited states of the two porphyrin macrocycles.[2,4] Excitonic interactions have also been claimed to be responsible for an extra band in the visible (called the Q′ band), at 15,620 cm^{-1}.[2,4] An extra band that appears at 21,413 cm^{-1} (Q") has been assigned to a porphyrin to Ce CT transition.[2,4]

Our calculated spectrum (Table III) is in good accord with experimental observations, but not necessarily with their interpretation.[2,4] The main UV-visible spectroscopic features are assigned to $\pi \rightarrow \pi^*$ transitions, comprised of orbitals delocalized over both porphyrin moieties.

For an appropriate interpretation of the spectra of the bisporphyrin sandwich complexes, we go back to Gouterman's four orbital model[39,40] that nicely explains the UV-visible spectroscopy of porphyrins and their derivatives, and extend it to the case of strongly coupled bisporphyrin systems. This model has been previously applied to describe the optical properties of sandwich complexes[7] and bacteriochlorin dimers.[15] For porphyrins with D_{4h} symmetry, the four MOs of Gouterman's model are the two highest occupied, of a_{1u} (π) and $a_{2u}(\pi)$ symmetry, and the two lowest empty of $e_g(\pi^*)$ symmetry. Configurations involving single excitations from the two occupied into the two empty yield two states of E_u symmetry with almost equal intensity. The optical spectrum is reproduced only when these two E_u configurations are allowed to undergo configuration interaction. Due to configurational mixing the higher energy Soret, or B band, contains nearly all the intensity, while the Q bands are weak. The energy and oscillator strength of the Q band from this model are generally predicted in an accurrate fashion. The B band is more complex, and higher excitations are required to yield energies in good accord with

excitations (CR, the special case of balanced CT with no net charge separation). This has been clearly shown for the calculated spectra of the magnesium bacteriochlorin dimer,[15] where the components of the Q band has been assigned, after CI calculations, to either Ex or CR transitions.

The accuracy of this resolution into monomer units can be checked by inspection of Table I. The ordering of the MOs is in accord with the EO model: the energies of $\tilde{D}_3(113)$ through $\tilde{D}_8(118)$ are calculated as predicted by the EO model. (The number in parentheses refers to the actual MO number in the calculation; see Fig. 2.) Although $\tilde{D}_2(112)$ is 97% D_2, D_1 contributes only 72% to $\tilde{D}_1(111)$. The quoted fractions are obtained by summing the squares of the coefficients on fragment MOs (72) and (180), Table I. It is this observation that will complicate the analysis of the spectrum in terms of the monomers. This mixing is not reduced upon separation of the rings to 4.0 Å. In this sense the analysis of the spectrum is *unlike* that of the dimer observed in photosynthesis, and this difference will prove important. The resolution of the lowest excited states in terms of the actual eight factor orbitals is given in Table IV.

There are 16 possible single excited configurations generated by means of transitions among the four HOMOs and four LUMOs of the EO manifold, that can be distinguished by their (x,y) polarization. Because they are equivalent under symmetry considerations, we will focus our discussion on the x-polarized contributions to each band. We have, in fact, considered a much larger orbital space, performing a CI calculation including 348 singly exited configurations from the INDO/S reference GS of $Ce(OEP)_2$. The resulting CI coefficients of the lowest lying states are dominated by excitations within the EO manifold, (Table III, IV). The exceptions are low lying $\pi \rightarrow$ Ce(f) excitations, the shoulder of the Soret band, and the Soret (B) band itself.

We have analyzed the Ex and CR contributions to the main features of the spectra in the framework of the coupled chromophore approach. The spin adapted determinants of all the single excited configurations from the EO manifold can be expressed in terms of these linear combinations of the monomer MOs (LCMOs), see Table V. The columns in Table V represent the

single determinant configurations of the dimer, and the rows the basis of monomer determinants. Due to the symmetry of the dimer, all single excited configurations are composed of equal contributions of monomer Ex and CT excitations, only the phases differ. We have expressed the INDO/S CI results in terms of monomer excitations by transforming the CI vectors in terms of these LCMO coefficients (see Table VI). The contribution from the EO model states is given in Table VI and deviations from 100% measure the limitation (or failure) of this model. As noted above, these deviations stem from contributions of other degenerate monomer orbital pairs to the states $\tilde{D}_i$ indicating a far more complex configurational mixing.

According to this analysis, Q′ and Q_0 are composed of equal contributions of Ex and CT excitations, i. e. the decomposition into two weakly interacting chromophores does not pertain for these two states. In the Q_1 region we calculate a CR state, as well as allowed $a_2(\pi) \rightarrow$ Ce (f) ligand-to-metal charge transfer excitations.

The label Q_1 is usually reserved for vibrational overtones of the Q_0 transition. The Q_0 excitation calculated here, however, is a true supermolecule excitation, and, according to Table IV, very unlike the Q_0 transition in a simple porphyrin. Nevertheless we cannot rule out contributions of vibrational Q_0 overtones to Q_1 which in related porphyrin systems are assumed to lie some 1200 cm^{-1} to 1500 cm^{-1} higher in energy. The shoulder 3,000 cm^{-1} to the blue of the Soret band (Fig. 3, Table III), is associated with $\pi \rightarrow \pi^*$ transitions from orbitals of e_2 symmetry of lower energy than those of the EO manifold, to the e_1, e_3 LUMOs. Intradimer CR configurations are expected to be higher in energy than the Ex ones.[15] Their relative contributions to the Q" and B bands are not insignificant and explain an energy lower than normally expected from coupled-chromophore model. The transitions we calculate in the Q_1 region have a large contribution of porphyrin-to-metal CT excitations.

With the aim of better understanding the nature of our results, and in order to associate the origin of the bands to a particular Ex or CR configuration, we have analyzed the effect of

increasing the interring separation. For a 4.0 Å separation between the N_p planes, the weaker $\pi \rightarrow \pi^*$ interaction allows a strong mixing of the f orbital of b_2 symmetry with the HOMO b_2 orbital that belongs to the EO manifold and the EO model is not directly applicable. The LUMO MOs retain the LCMO description similar to the more strongly perturbed case of the closely placed porphyrin rings. The orbital of the EO model that belong to linear combinations of a_{1u}, a_{2u}, and e_g orbitals of the monomers can be identified, but there is a strong contribution of $\pi \rightarrow$ f transitions to the excitations. The Q′ and Q_0 transitions remain $\pi \rightarrow \pi^*$ and can be compared to those obtained for the experimental interring separation. Although a larger number of configurations contribute to each band, they can be analyzed as a near 50%–50% mixture of Ex and CR configurations when expressed in terms of the orbitals of the monomer. In agreement with the results derived for the shorter interring separation, Q′ and Q_0 remain true supermolecule states.

We have also imposed an electric field of $3x10^{-4}$ au perpendicular to the N_p planes (1 au = $5.14x10^{11}$ V/m). As can be demonstrated using first order perturbation theory,[15] small changes in the CI vectors are associated with Ex configurations, while those that describe CR configurations change significantly under the influence of the field. Inspection of the CI vectors of the Q′ and Q_0 bands shows that, out of the four configurations that define the bands, two have changed while two remain almost equal (Table VII examines the case for 4 Å). With this small field, the transition energies are almost unchanged, but the Q′ band borrows some intensity from allowed transitions. This analysis confirms our previous conclusion, showing that both Ex and CR configurations contributes to both the Q′ and Q_0 bands.

Although it is tempting to simplify the interpretation of this spectrum in terms of two monomers, the great degree of CR and Ex mixing in all our calculations seems to suggest this is not admissable. The Ce(IV) dimer, even at the larger separations, is acting as a true supermolecule with its own delocalized molecular orbitals, that even upon localization do

not yield a simple interpretation of the spectrum. This is a very different situation than that found for the chlorophyll special pair in the photosynthetic reaction center.[15] In this case two Mg-chlorophylls overlap only over one pyrrole ring (they are slipped from the face to face configuration here), and transitions are easily identified as either Ex or CR.

The UV-visible absorption spectrum of the oxidized molecule, $[Ce(OEP)_2]^+$, shows several features that are typical of the $[Ln(III)(OEP)_2]$ series (Fig. 5). They are characterized by a broad band in the Soret region and low intensity bands in the low energy region that are labelled as Q bands in analogy with the spectrum of the neutral species, together with a strong band in the NIR region. The assignment of the NIR band has been the subject of extensive research. The NIR band is absent in porphyrin π radicals and occurs only upon dimerization: they are a characteristic of electron deficient sandwich systems.[5] The transition energy of this band decreases as the ionic radius of the trivalent ion increases.[3,9] Initially this transition was described as an internal CT band from a porphyrin dianion, acting as a donor, to a porphyrin monocation radical that acts as the acceptor.[4] Resonance Raman measurements suggests that the electron vacancy is completely delocalized on both vibrational and electronic time scales, and the transition more likely implies π orbitals delocalized over the entire system.[6] This is in agreement with our calculations and in agreement with our findings that this system is more one molecule than two that are weakly coupled.

We calculate three bands in the near infra-red region, Table VIII. The most important of these is the allowed transition $^2B_1(b_1 \rightarrow a_2)$, calculated at 7973 cm^{-1}, to be compared to the experimental value of 7874 cm^{-1}. This transition $\tilde{D}_3 \rightarrow \tilde{D}_4$ is of CR type, containing an equal mix of $A_2 \rightarrow B_2$ and $B_2 \rightarrow A_2$, see Figure 4. This balanced mixture, however, is easily affected by an electric field. A field of 10^{-4}au creates new orbitals, $\tilde{D}_3 = 0.76A_2 + 0.65B_2$ and $\tilde{D}_4 = 0.65A_2 - 0.76B_2$, and leads to the electronic charge transfer of 0.13 au from one macrocyle to the other in the ground state and an opposite charge transfer in the first excited (NIR) state. This is

easily seen from an inspection of the corresponding Mulliken results. Whereas the charge of the Ce atom remains unaffected in all cases (1.84 au), the charges of the macrocyle ligands change from q(A) = q(B) = 0.42 au to q(A) = 0.55, q(B) = 0.29 au in the ground state and to q(A) = 0.29, q(B) = 0.55 au in the first excited (NIR) state due to the electric field. It is interesting to speculate on the importance of this charge transfer in the context of the observed conductivity.

According to our calculations (Table VIII), the NIR band involves a transition from the highest completely filled orbital to the half-filled HOMO a_2 (Fig. 2). This promotion of an electron represents an allowed transition in D_{4d} for z polarization. As the distance between the monomers increases, the splitting of the dimer's MO $\tilde{D}_3(b_1)$ and $\tilde{D}_4(a_2)$ decreases. This has an important effect on the position of the NIR band, explaining the shift to lower energy as the ionic radii of the central ion increases.

In addition to the Soret and NIR bands, there is a band of low intensity at 19,455 cm^{-1} (Fig. 5). Although not always reported,[4,6] a small shoulder around 15,500 cm^{-1} can also be identified. Because the nature of the MOs of the EO manifold is the same as in the neutral species, the bands in the neutral molecule and in the positively charged dimer can be related on the basis of their electronic assignments. We assign the 15,500 cm^{-1} "Q_0 band" to two transitions (Q_{0a}, Q_{0b}, Table VIII). The more intense of these complies with the EO model, the other, weaker, calculated at 17,442 cm^{-1} does not. The band at 19,455 cm^{-1}, blue shifted relative to the Q_1 band of the neutral, is assigned also to two calculated transitions, one of which is $\pi \rightarrow$ Ce(f). A Q" band is calculated at the same energy as in the neutral molecule and has the same composition. This band is not reported experimentally. It might be hidden under the Soret band which is much broadened in the ion. There are also several transitions of low intensity calculated to lie between the Q" and the Soret bands, for both the neutral and the cationic species (Tables III, VIII), that are associated with $\pi \rightarrow$ f charge transfer transitions and that would be expected to contribute to the intensity and broadness of the B band. This effect would be even larger in

the spectrum of the cation, where promotions of inner electrons to the half-filled HOMO also result in transitions calculated to lie in this energy region. In agreement with experiment, the Soret band is blue shifted relative to the neutral, with a shoulder 2,300 cm^{-1} to the blue.

The occurrence of the NIR band, together with the shifting of the "Q'" bands, are not the only effects that follow the creation of an electron vacancy in the HOMO to give a half-filled orbital. In the ground state of the cation dimer the net bonding between the two porphyrin macrocycles is increased because the antibonding HOMO a_2 is now singly occupied. This difference in bond order of 0.5 (see Table II) leads to a smaller interring separation. In agreement with this inference, we have found a better description of the electronic spectrum of the cation for an interring separation which is 0.2 Å shorter than that of the neutral dimer. Blue shifting of the bands relative to the neutral counterparts can be associated, at least partially, to the greater interring interaction.

In assigning the bands in Table VIII we again make use of a fragment analysis, and the Stark effect. The calculated results for the Stark effect appear in Table IX for the case of 4 Å separation case which is slightly easier to analyze. Due to the fact that the applied field destroys the reflection plane, states of E_3 symmetry gain some intensity at the expense of the E_1 manifold. Again, the Soret band is complicated by a large number of transitions involving orbitals outside the EO manifold. Although involving the same orbitals as in the neutral species, only the Q_0 band retains its mixed Ex-CT character in the cation. The Q_1, Q" and B bands, previously described as CR, Ex and Ex, respectively, are associated, in the cation, with Ex, CR, and mixed bands. In other words, it may not be useful in comparing this spectrum with that of the neutral.

3.2 $Eu(OEP)_2$

3.2a Ground state calculations $Eu(OEP)_2$ is known to be paramagnetic,[5] with a magnetic moment of 3.55 μB at 302 K that falls to 1.28 μB at 26 K. Possible formulas are represented

by $Eu^{+2}(OEP)_2^{-2}$, $Eu^{+3}(OEP)_2^{-3}$, or $Eu^{+4}(OEP)_2^{-4}$. The first implies a larger number of unpaired electrons on the central atom (f^7), together with two radical porphyrin monoanions, Eu(II) $(OEP)_2$, the second implies an f^6 electronic configuration on the central atom, and an unpaired electron on the macrocycle rings associated either with a localized model, as $Eu(III)(OEP)^{-2}(OEP)^{-}$, or with a delocalized unpaired electron on both macrocycles. The last possible structure, $Eu(IV)(OEP)_2$, has each OEP with a charge –2, typical for most transition metal porphyrin systems. Because the two radical spins may be quenched by spin pairing of the cofacial radical systems,[41] the experimental determination of the magnetic moment is not enough to assign the proper oxidation state to the central atom. A Mulliken population analysis has been performed to this end after MRCI calculations, comparing the stability of the different multiplicities that are compatible with the open shell electronic configuration. The MO description is considerably more complicated than that of $[Ce(OEP)_2]^+$, due to the filling of the f orbitals, which stabilizes high spin configurations and brings about serious convergency problems. The most ready convergence was obtained by assigning six electrons to the seven f orbitals, and one to the orbital a_2, see Figure 6, and by assuming a multiplicity m = 8. The resulting orbitals were used for the subsequent CI calculations, which are consistent with this assignment. We have found a population of 6 electrons in the f orbitals for the lowest energy states of multiplicities m = 4 through 10, which is indicative of an oxidation state III on the central metal atom. On the basis of the previous discussion, centered on the $[Ce(OEP)_2]^+$ molecule (section 3.1-a), we represent the structure as $Eu(III)(OEP)_2^{-3}$ because, as in the case of Ce, the equivalent Mulliken populations on both moieties indicate a delocalization of the electronic vacancy over the entire π system, even after modest geometric distortions that destroy the equivalence of the rings. The electronic configurations, $s^{0.43}p^{0.97}d^{2.12}f^{6.10}$ (m = 4, 6), $s^{0.43}p^{0.95}d^{2.03}f^{6.08}$ (m = 8), and $s^{0.43}p^{0.97}d^{2.83}f^{6.08}$ (m = 10), show a back donation effect from the ligands to the d orbitals, resulting in a occupation of the $d(z^2)$ orbital.

Including all the possible ways of occupying the f orbitals for the definition of the reference states (i. e. 21 references for the octet), MRCI calculations show that the GS is an octet, $^8E_3$, in D_{4d} symmetry. This state is nearly degenerate with a $^6E_3$ state in which there is anti-ferromagnetic coupling between the metal and the ligands, calculated 11 cm^{-1} higher in energy. Given that lowering the temperature decreases the magnetic moment, the calculated order of these states is probably reversed. Both $^8E_3$ and $^6E_3$ have low lying f $\rightarrow$ f transitions, $^8A_2$, $^8E_2$ and $^8E_1$, (and $^6A_2$, $^6E_2$ and $^6E_1$) calculated at 60 (61) cm^{-1}, 114 (145) cm^{-1} and 313 (320) cm^{-1}, respectively. Recall that KT at room temperature is 210 cm^{-1}. States of higher and lower multiplicity are calculated considerably higher in energy; the former requires a further ligand-to-metal charge transfer, the latter a spin-flip on the metal and loss of considerable exchange energy. All of these findings are consistent with an f^6 configuration on the central atom. Six unpaired electrons on the central atom, together with the radical ligand, ferromagnetically coupled, yield a multiplicity of 8, whereas anti-ferromagnetic coupling yields a multiplicity of 6.

The π orbitals of the EO manifold retain the same characteristics as in the analoguous Ce compound, and can be described as a linear combination of MOs on the monomers, with electron density on the C_α and C_β atoms of the pyrrole rings in the b_1 and a_2 orbitals (linear combination of a_{1u} orbitals of the monomers), and on the N_p atoms on the b_2 as well as the a_1 orbitals (linear combination of monomer orbitals of a_{1u} symmetry). Metal centered d orbitals are mixed with the π orbitals in setting up the frontier orbitals, while the f orbitals, partially filled, lie lower in energy.

3.2b UV-visible spectroscopy The lowest state of the radical ligand in this picture is a doublet. The introduction of a paramagnetic ion, a septet state, as is the case of f^6 Eu(III), causes spin coupling with the diporphyrin π states. The possible states generated from the dimer $(OEP)_2^{-3}$ are doublets and quartets. We have found the ground state to be an octet, coupling the metal-

septet to the ligand doublet. Both excited doublets (coupled to the metal to be octets or sextets) and quartets (coupled to dectets, octets, sextets, and quartets) of the ligand system generate spin-allowed octets, [36] called doub-octets, and quart-octets, [42] respectively. We note that the calculated spectroscopy does not change significantly if we assume a ground state sextet, as the metal ligand coupling seems reasonably weak. (The largest difference for all states below 15,000 cm^{-1} is 170 cm^{-1}.) Indeed, our calculated spectrum assuming the doub-octet ground state for $Eu(III)(OEP)_2^+$, is not much different from that obtained for the doublet $Ce(IV)(OEP)_2^+$, with the exception of the allowed, but weak quart-octets in the former case. The calculations on $Eu(III)(OEP)_2^+$ are, however, further complicated as there are seven almost degenerate octet states, originating from the different ways to accomodate the six electrons within the f shell, that compete for the definition of the initial state, especially at elevated temperatures. The transition energies in the UV-visible region of the spectrum calculated from these other low lying states are not expected to change significantly, but their intensities might. We have not been abie to perform calculations including the spin-orbit coupling of the lowest octet to the sextet states because of the size of the matrices generated when these multiplicities are involved. An appropriate modification of the computer code is in progress.

The resulting spectrum (Table X) shows several similarities to that of $[Ce(OEP)_2]^+$. $f \rightarrow \pi$ transitions begin to appear around 24,500 cm^{-1}. The bands in the spectrum can be labelled in a similar fashion as those of $[Ce(OEP)_2]^+$, because they involve transitions between orbitals of the same type. Features at 14,900 and 17,200 cm^{-1}, calculated at 15,297 and 17,209 cm^{-1}, respectively, are associated with the two contributions of the Q_0 band, that are clearly resolved in the spectrum of $Eu(OEP)_2$. The calculated Q_1 band is red shifted relative to the Ce cation, in agreement with the experimental data. The Q" band, not visible for the Ce cation dimer, but hidden under the broad Soret band, becomes discernable in the Eu dimer as a feature at 20,408 cm^{-1}, due to the shift to lower energies. The red shift of the bands can be rationalized through

the smaller HOMO-LUMO gap and the smaller energy differences among the orbitals involved in the transitions after somewhat stronger mixing with the metal d orbitals (Fig. 6).

The NIR band deserves further discussion. In recent RR spectroscopic studies at high resolution and low temperature (10 K),[6] a well resolved fine structure was observed in the Eu NIR band, which was shown to extend from 7,800 to 9,200 cm^{-1}, with maxima around 8,500 cm^{-1}. A similar result was found for the Ce cation complex[6] which shows features that extend to 10,200 cm^{-1} in the high energy region. Our calculations produce three main features around 7,800, 8,500, and 9,200 cm^{-1} for the Eu complex, and 7,800, 9,700, and 10,400 cm^{-1} for the Ce cationic complex. Although only one of these transitions is calculated as allowed on the basis of symmetry considerations, the importance of vibronic structure in the definition of the NIR band allows us to associate these observations to three calculated components, which involve transitions from the fully occupied orbitals $\tilde{D}_1$, $\tilde{D}_2$, and $\tilde{D}_3$ to the singly occupied HOMO $\tilde{D}_4$. According to the model of Piepho,[43] applied to sandwich porphyrines, linear combination of A_{2u} (in D_{4h} symmetry) out-of-plane deformations of the monomeric units exhibit the appropriate symmetry to provide vibronic activity in the intradimer CT transition. A symmetric linear combination of such modes, Q, yields an A_{1g} (A_1 in D_{4d} symmetry) Franck-Condon active dimer vibration. On the other hand, the asymmetric linear combination, Q_- results in an A_{2u} (B_2 in D_{4d} symmetry) pseudo Jahn-Teller active mode which couples the two zero-order electronic states. The multicenter mode, Q_{ab}, in the sandwich complexes can be viewed as a Franck-Condon active A_{1g} (A_1 in D_{4d}) pure dimer vibration that modulates the interring separation. When strong overlap and substantial delocalization occurs, Q_{ab} is expected to dominate, giving a symmetrical band shape.

The different possible ways of accommodating the unpaired electrons in the f orbitals, together with the mixing of the e_2 d metal orbitals with the frontier π orbitals of the ligand (see Fig. 6), complicates the description of the CI vectors for the $Eu(OEP)_2$ molecule, which

have, in some cases, contributions from over 20 configurations. These configurations relate back to those found in the more simple EO model after symmetry is taken into account.

4. CONCLUSIONS

In this paper we have examined the electronic structure of several bisporphyrine compounds, $Ce(OEP)_2$, $Ce(OEP)_2^+$, and $Eu(OEP)_2$. Although there is quite a bit of ligand-to-metal back donation in the two Ce complexes (the Mulliken population suggests Ce is +1.84 in both), the cerium atom is best characterized as Ce(IV). In the corresponding cation the electron "hole" is distributed equally between the two porphyrin macrocycles. The calculated UV-visible spectra are in good accord with experiment. The near IR band in the cation (NIR) is calculated to be composed of three transitions, only one of which carries oscillator strength. This latter transition is found to be nearly pure where an electron is promoted from the second highest fully occupied orbital, b_1, to the half-filled HOMO, a_2. When decomposed in terms of the eight-orbital (EO) model, it is found to be of charge resonance character (CR). A small electric field breaks the symmetry between the two macrocycles and leads to a charge asymmetry in both ground state and the allowed NIR final state.

We find the ground state of $Eu(OEP)_2$ to be best described as $^8E_3$, a state with six f electrons, all of the same spin direction, but with a single electron split between the $f(xz^2)$ and $f(yz^2)$ atomic orbitals. Very close in energy (11 cm^{-1}) lies a state of $^6E_3$ symmetry, representing antiferromagnetic coupling between the f^6 metal ion $Eu^{+3}$and the ligand radical $(OEP)_2^{-3}$. Also close in energy lie states with other f orbital occupancies, of A_2, E_2 and E_1 symmetry. Occupation of these states, both as octets and sextets would be expected to further broaden the spectrum. The description of both the ground and excited states of $Eu(III)(OEP)_2$ that we calculate are very similar to those of $Ce(IV)(OEP)_2^+$.

The observed spectra of the lanthanide bisporphyrinate complexes do resemble in some sense the spectra of porphyrins themselves, and they can, to a large degree, be interpreted in an EO model, a natural extension of Gouterman's four–orbital model,[39,40] a model that has been used very successfully in analyzing the spectrum of the chlorophyll dimers observed in the reaction center of photosynthetic bacteria.[15,44] But the similarity of the lanthanide double decker systems to this chlorophyll dimer is very limited. In the reaction center the two chlorophyll molecules overlap in one ring only, the mean distance between planes is 3.3 Å, and the coupling is very weak. The coupled-chromophore model works well if we extend it to include charge transfer (CT) as well as excitonic (Ex) coupling. In the lanthanide sandwich compounds, the two porphyrin macrocycles are over one-another and staggered and they have interring contacts as small as 2.8 Å. The coupling, both direct and through the lanthanide ion, is strong. States are not described easily as Ex or CT, and we find the Q-B notation used to describe porphyrin spectroscopy both confusing and misleading. These complexes behave as true supermolecules, and their excited states deserve their own unique notation.

Acknowledgment This work was supported in part through grants from the Consejo Nacional de Investigaciones Científicas y Técnicas (CONICET), from the Fundación Antorchas (República Argentina), from the Office of Naval Research, and from the Fonds der Chemischen Industrie. M.C.Z. is grateful to the Alexander von Humboldt Foundation for support while in Germany. During this stay important tools for the present investigation were developed.

14. Scherer, P. O. J; Fischer, S. F. *Chem. Phys.* 1989, 131, 115-127.

15. Thompson, M. A.; Zerner, M. C.; Fajer, J. *J. Phys. Chem.* 1990, 94, 3820-3828.

16. Girolami, G. S.; Milam, S. N.; Suslick, K. S. *J. Am. Chem. Soc.* 1988, 110, 2011-2012.

17. Buchler, J. W.; de Cian, A.; Fischer, J.; Hammerschmitt, P.; Weiss, R. *Chem. Ber.* 1991, 122, 2219-2228.

18. Cho, S.-H.; Kim, H.-J.; Kim, H.; Lee, W.; Gorlin, P. A.; Girolami, G. S.; Suslick, K. S. *Inorg. Chem.* 1991, 30, 2652-2656.

19. Martin, P. C.; Arnold, J.; Bocian, D. F. *J. Phys. Chem.* 1993, 97, 1332-1338.

20. Stichternath, A.; Schweitzer-Stenner, R.; Dreybrodt, W.; Mak, R. S. W.; Li, X.; Sparks, L. D.; Shelnutt, J. A.; Medforth, C. J.; Smith, K. M. *J. Phys. Chem.* 1993, 97, 3701-3708.

21. a) Sparks, L. D.; Medforth, C. J.; Park, M. S.; Chamberlain, J. R.; Ondrias, M. R.; Senge, M. O.; Smith, K. M.; Shelnutt, J. A. *J. Am. Chem. Soc.* 1993, 115, 581-592. b) Sparks, L. D.; Anderson, K. K.; Medforth, C. J.Smith, K. M.; Shelnutt, J.A. *Inorg. Chem.* 1994, 33, 2297-2302.

22. Pople, J. A.; Santry, D. P.; Segal, G. A. *J. Chem. Phys.* 1965, 43, S129.

23. Pople, J. A.; Beveridge, D. L.; Dobosh, P. A. *J. Chem. Phys.* 1967, 47, 2026.

24. Zerner, M. C. ZINDO package, Quantum Theory Project, Williamson Hall, University of Florida.

25. Ridley, J.; Zerner, M. C. *Theor. Chim. Acta* 1973, 32, 111-134.

26. Ridley, J.; Zerner, M. C. *Theor. Chim. Acta* 1976, 42, 223.

27. Zerner, M. C.; Loew, G.; Kirchner, R.; Mueller-Westerhoff, U. *J. Am. Chem. Soc.* 1980, 102, 589-599.

28. Du, P.; Axe, F. U.; Loew, G. H.; Canuto, S.; Zerner, M. C. *J. Am. Chem. Soc.* 1991, 113, 8614-8621.

29. Kotzian, M.; Rösch, N.; Zerner, M. C. *Theor. Chim. Acta* 1992, 81, 201-222.

B. FIGURE CAPTIONS

Figure 1- Geometry of the $Ce(OEP)_2$ molecule. Ethyl radicals are not included, as they are not taken into account in the calculations (see text). Mutually perpendicular views show: a) The staggered geometry. b) The doming of the porphyrin rings when coordinated to the central lanthanide ion.

Figure 2- MO diagram for $Ce(OEP)_2$ and $[Ce(OEP)_2]^+$. The orbitals are labelled according to D_{4d} symmetry. The four highest occupied and four lowest unoccupied MOs of the dimer, (see also Fig. 4), are the basis for the eight-orbital model as discussed in the text. They are composed of linear combination of the porphyrin monomer orbitals.

Figure 3- UV-visible spectrum of $Ce(OEP)_2$. Q and Soret bands are shown. With permission of Donohoe et al. (ref. 4).

Figure 4-MOs of the eight-orbital model of the dimer in terms of their monomers constituents. For the dimer orbitals D_i the sign of the linear combination of the monome orbitals is given as is the irreducible representation of group D_{4d}. The D_{4h} symmetry labels for the monomer orbitals are shown for convenience.

Figure 5- Optical absorption spectra of the electron deficient complexes $Ce(OEP)_2^+$ and $Eu(OEP)_2$, compared to the spectrum of $Ce(OEP)_2$. Q, Soret and NIR bands are indicated. a) UV/vis range. b) near IR range. With permission of Buchler et al. (ref. 5).

Figure 6- MO diagram for $[Eu(OEP)_2]$ at the experimentally observed interring separation. The orbitals are labelled according to D_{4d} symmetry. Low lying f orbitals are partially filled (see text).

Table I : Analysis of the frontier molecular orbitals in terms of the fragments. AO labels 1-16 are Ce based ao's: 1 f(z^3), 2 f(xz^2), 3 f(yz^2), 4 f($z(x^2-y^2)$), 5 f(xyz), 6 f(x^3-3xy^2), 7 f($3yx^2-y^3$), 8 d(z^2), 11 d(xz), 12 d(yz). Fragment orbitals 17-125 are upper porphyrin based (A), while 126-234 are lower porphyrin based (B). Fragment orbital 73 is the HOMO (a_{1u}) of A, 181, the HOMO (a_{1u}) of B, etc. (see also figure 2)

2.8Å

MO.	E(a.u.)	A	B	Ce
107 e3	-0.324	0.64(70)+0.24(66)	+0.64(178) + 0.24(174)	
108	-0.324	0.64(71)+0.24(65)	+ 0.64(179)+ 0.24(173)	
109 e1	-0.316	0.65(70)+0.22(66)	-0.65(178) - 0.22(174)	
110	-0.316	0.65(71)+0.22(65)	-0.65(179) - 0.22(173)	
111 a1=$\tilde{D}$1	-0.252	0.60(72)+0.31(68)	+0.60(180) + 0.31(176)	+0.25(8)
112 b2=$\tilde{D}$2	-0.247	0.69(72)+0.13(68)	- 0.69(180) - 0.13(176)	
113 b1=$\tilde{D}$3	-0.235	0.71(73)	+0.71(181)	
114 a2=$\tilde{D}$4	-0.210	0.71(73)	- 0.71(181)	
115 e3=$\tilde{D}$5	-0.050	0.69(74)	+0.69(182)	
116 $\tilde{D}$6	-0.050	0.69(75)	+0.69(183)	
117 e1=$\tilde{D}$7	-0.042	0.69(74)	-0.69(182)	+0.10(2)
118 $\tilde{D}$8	-0.042	0.69(75)	-0.69(183)	+0.10(3)
119 to 125	-0.010 to -0.007	-	-	0.99 (f)

4.0Å

MO.	E(a.u.)	A	B	Ce
107 e3	-0.326	0.69(70)+0.12(64)	+0.69(178) + 0.24(172)	0.09(11)
108	-0.326	0.69(71)+0.12(65)	+ 0.69(179)+ 0.12(173)	0.09(12)
109 e1	-0.323	0.65(70)+0.22(64)	- 0.65(178) - 0.22(172)	
110	-0.323	0.65(71)+0.22(65)	-0.65(178) - 0.22(173)	
111 a1=$\tilde{D}$1	-0.244	0.60(72)+0.31(68)	-0.60(180) - 0.31(176)	+0.25(8)
112 b2=$\tilde{D}$2	-0.243	0.69(72)+0.13(68)	+0.69(180) + 0.13(176)	
113 b1=$\tilde{D}$3	-0.223	0.71(73)	+0.71(181)	
114 a2=$\tilde{D}$4	-0.221	0.71(73)	- 0.71(181)	
115 to 121	-0.099 - to -0.082	-	-	0.99 (f)
122 e3=$\tilde{D}$5	-0.047	0.68(74)	+0.68(182)	+0.17(11)
123 $\tilde{D}$6	-0.047	0.68(75)	+0.68(183)	+0.17(12)
124 e1=$\tilde{D}$7	-0.045	0.69(74)	-0.70(182)	
125 $\tilde{D}$8	-0.045	0.69(75)	-0.70(183)	

Table II: Fragment Analysis of Ce(IV)(OEP)2 and Ce(IV)(OEP2)+ at 2.8Å. Fragment 1 is Ce(IV), fragments 2 and 3 are the OEP's.

Ce(IV)(OEP)2				Ce(IV)(OEP2)+		
INTERFRAGMENT CHARGE AND BOND ORDER						
	1	2	3	1	2	3
1	3.633			3.620		
2	14.584	112.184		14.595	111.690	
3	14.584	2.695	112.184	14.595	3.368	111.690
INTERFRAGMENT MULLIKEN ANALYSIS						
	1	2	3	1	2	3
1	1.779			1.768		
2	0.419	112.704		0.413	112.208	
3	0.419	-0.025	112.704	0.413	-0.009	112.208
INTERFRAGMENT BOND INDEX						
	1	2	3	1	2	3
1	0.000			0.000		
2	2.907	0.000		2.900	0.000	
3	2.907	0.190	0.000	2.900	0.689	0.000
Ce(IV) FRAGMENT						
f:	0.129			0.138		
d:	2.200			2.179		
s:	0.409			0.405		
p:	0.894			0.884		

Table III: INDO/S-CI calculated excited states of neutral [Ce(OEP)$_2$]. Only the CI coefficients of states reached by xz polarization are given.

State	Dominant configuration	CI coeffient		Δ E [cm^{-1}]	Oscillator strength	ΔE_{exp} [a)] [cm^{-1}]	
$^1E_3$	$a_2 \rightarrow e_3$	-0.92		13610	0.000	15390	Q′, Ex/CR
$^1E_1$	$b_2 \rightarrow e_3$	-0.45		15280	0.274	17452	Q_0, Ex/CR
	$a_2 \rightarrow e_1$	-0.78					
$^1B_1$	$a_2 \rightarrow b_2$	1.00		17157	0.000	–	$\pi \rightarrow$ f
$^1E_3$	$a_2 \rightarrow e_3$	0.99		17245	0.000	–	$\pi \rightarrow$ f
$^1E_2$	$a_2 \rightarrow e_2$	1.00		17323	0.000	–	$\pi \rightarrow$ f
$^1E_1$	$a_2 \rightarrow e_1$	0.96		17604	0.008		$\pi \rightarrow$ f
$^1E_1$	$b_1 \rightarrow e_3$	-0.79		19407	0.001	18870[b)]	Q_1[b)], CR
	$a_2 \rightarrow e_1$	-0.47					
$^1E_1$	$b_2 \rightarrow e_3$	0.91		21680	0.041		$\pi \rightarrow$ f
$^1B_2$	$a_1 \rightarrow b_2$	0.97		22106	0.016	–	$\pi \rightarrow$ f
$^1E_1$	$a_1 \rightarrow e_1$	0.91		22171	0.004	–	$\pi \rightarrow$ f
$^1E_1$	$b_1 \rightarrow e_3$	0.99		22599	0.001	–	$\pi \rightarrow$ f
$^1E_1$	$a_2 \rightarrow e_1$	0.63		24271	0.099	21413	Q″, Ex
	$b_2 \rightarrow e_3$	0.64					
$^1E_1$	$a_1 \rightarrow e_1$	0.53		32310	5.800	26455	B, Ex
	$b_2 \rightarrow e_3$	-0.34					
	$b_1 \rightarrow e_3$	-0.39					
$^1E_1$	$e_2 \rightarrow e_1$	0.33	c)	35976	2.432	27500	$\pi \rightarrow \pi^*$
	$e_2 \rightarrow e_3$	0.46					

a) Ref. 4.

b) In this region is also the vibrational overtone of the Q_0, called Q_1, see text. Only states with calculated oscillator strengths are reported above 20 000 cm^{-1}.

c) These are pairs of these e $\rightarrow$ e excitations, each with coefficients as given.

Table IV: CI coefficients for the xz type states of Ce $(OEP)_2$ at the experimental separation. Note that these coefficients are for the actual orbitals of Table I, not the idealized eight-orbital model, Figure 4.

	Q′	Q_0	Q_1	Q″	B
$\tilde{D}_4 \rightarrow \tilde{D}_5$	-0.92	0.00	0.00	0.00	0.00
$\tilde{D}_2 \rightarrow \tilde{D}_6$	0.00	-0.45	0.00	-0.62	-0.34
$\tilde{D}_4 \rightarrow \tilde{D}_7$	0.00	-0.78	0.47	0.00	0.00
$\tilde{D}_3 \rightarrow \tilde{D}_5$	0.00	0.00	-0.79	0.00	-0.38
$\tilde{D}_1 \rightarrow \tilde{D}_8$	0.00	0.00	0.00	-0.63	0.53
eight-orbital	85%	81%	85%	81%	55%

Table VI: Description of the excited states of Ce $(OEP)_2$ at the experimental geometry in terms of local excitations. Only x components are given; the y components are identical.

	Q′	Q_0	Q_1	Q″	B
$A_2 \rightarrow A_3$	0.46	0.38	-0.16	0.00	-0.19
$B_2 \rightarrow A_3$	0.46	0.38	0.60	0.00	0.19
$A_2 \rightarrow B_3$	0.46	-0.38	-0.60	0.00	-0.19
$B_2 \rightarrow B_3$	0.46	-0.38	0.16	0.00	0.19
$A_1 \rightarrow A_4$	0.00	0.21	0.00	-0.56	0.37
$B_1 \rightarrow A_4$	0.00	-0.21	0.00	0.02	0.05
$A_1 \rightarrow B_4$	0.00	0.21	0.00	-0.02	-0.05
$B_1 \rightarrow B_4$	0.00	-0.21	0.00	0.56	-0.37
eight-orbital	85%	76%	77%	64%	43%
CR	50%	50%	94%	0%	18%

a) Note that these values are different from those that appear in Table VI as they refer to a projection on the MOs D_i (see Table VII) and not the orbitals $\tilde{D}_i$ of Table I.

Table VII: Changes in the calculated INDO/S CI coefficients, transition energies ΔE [cm^{-1}] and oscillator strengths f for the low energy Q bands of Ce $(OEP)_2$ under the influence of an applied field F (10^{-4}au). The interring separation is 4 Å.

	Q′		Q_0		
F	0	10^{-4}	0	10^{-4}	
$a_1 \rightarrow e_3$	0.398	0.424			Ex
$b_2 \rightarrow e_1$	-0.392	0.360			Ex
$b_1 \rightarrow e_1$	-0.532	-0.402			CR
$a_2 \rightarrow e_3$	-0.634	-0.491			CR
$a_1 \rightarrow e_1$			-0.420	0.318	CR
$b_2 \rightarrow e_3$			0.486	-0.388	CR
$b_1 \rightarrow e_3$			0.554	-0.506	Ex
$a_2 \rightarrow e_1$			0.528	-0.563	Ex
ΔE [cm^{-1}]	15560	15559	15739	15743	
f	0.000	0.001	0.219	0.109	

Table VIII: INDO/S-CI calculated excited states of the cation $[Ce(OEP)_2]^+$. Only the xz polarized CI coefficients are given, for the yz polarized differ only in phase.

State	Dominant conf. CI coeff.	ΔE [cm^{-1}]	f	ΔE_{exp} [a)] [cm^{-1}]	Comments
$^2B_1$	$b_1 \rightarrow a_2$, 0.990	7973	0.2322	7874	NIR, CR
$^2B_2$	$b_2 \rightarrow a_2$, 0.990	9714	0.0000	—	
$^2A_1$	$a_1 \rightarrow a_2$, 0.990	10430	0.000	—	
$^2E_1$	$a_2 \rightarrow e_1$, 0.847 $b_1 \rightarrow e_3$, 0.338	12236	0.052	~15000	Q_{0a}, CR(Ex) Q_{0b}, Ex
$^2E_1$	$b_2 \rightarrow e_3$, 0.739 $a_1 \rightarrow e_1$, 0.425	17442	0.009		
$^2E_1$	$b_2 \rightarrow e_3$, 0.432 $b_1 \rightarrow e_3$, 0.915	18928	0.053	19455	Q_1, Ex
$^2E_1$	$a_2 \rightarrow e_1$, 0.988	20254	0.001		$\pi \rightarrow f$
$^2E_1$	$b_1 \rightarrow e_3$, 0.976	22856	0.002	—	$\pi \rightarrow f$
$^2E_1$	$e_1 \rightarrow a_2$, 0.670 $b_2 \rightarrow e_3$, 0.659	23264	0.036	—	$\pi \rightarrow \pi^*$
$^2E_1$	$a_1 \rightarrow e_1$, 0.789 $b_2 \rightarrow e_3$, 0.620	24109	0.061	23800	Q'', CR
$^2E_1$	$b_2 \rightarrow e_3$, 0.998	25102	0.034	—	$\pi \rightarrow f$
$^2B_2$	$a_1 \rightarrow b_2$, 0.990	25333	0.005	—	$\pi \rightarrow f$
$^2E_1$	$b_2 \rightarrow e_3$, 0.970	25395	0.012	—	$\pi \rightarrow f$
$^2B_2$	$a_1 \rightarrow b_2$, 0.980	25851	0.008	—	$\pi \rightarrow f$
$^2E_1$	$a_1 \rightarrow e_1$, 0.991	26546	0.051	—	$\pi \rightarrow f$
$^2E_1$	$e_1 \rightarrow a_2$, 0.712 $b_2 \rightarrow e_1$, 0.419	27509	0.045	—	$\pi \rightarrow \pi^*$
$^2E_1$	$a_2 \rightarrow e_1$, 0.359 $b_1 \rightarrow e_3$, 0.712	27995	0.065	—	$\pi \rightarrow \pi^*$
$^2E_1$	$b_1 \rightarrow e_3$, 0.969	33168	0.043	—	$\pi \rightarrow f$
$^2B_2$	$e_1 \rightarrow e_3$, 0.683	33357	0.023	—	$\pi \rightarrow \pi^*$
$^2B_2$	$e_1 \rightarrow e_3$, 0.531	34561	0.043	—	$\pi \rightarrow \pi^*$
$^2E_1$	$a_1 \rightarrow e_1$, 0.405 $e_2 \rightarrow e_3$, 0.311 $b_1 \rightarrow e_3$, 0.331	35553	4.532	27800	B, CR(Ex)
$^2E_1$	$e_2 \rightarrow e_1$, 0.312 $e_2 \rightarrow e_3$, 0.567	37882	2.395	30000	$\pi \rightarrow \pi^*$

a) Ref. 5.

Table IX: Changes in the calculated INDO/S CI coefficients, transition energies (ΔE [cm^{-1}]) and oscillator strengths f for the Q and Soret bands of the $[Ce(OEP)_2]^+$ electronic spectrum under the influence of an applied field. The monomers are separated by 4 Å. The first line gives the "in vacuo" value, while the second and third give the values obtained with applied fields of 10^{-4} and 10^{-3} au, respectively.

	Q_{0a}	Q_{0b}	Q_1	Q''	B
	–0.715				
$a_2 \rightarrow e_1$	–0.713				
	–0.608				
	–0.545	–0.481	0.672		0.321
$b_1 \rightarrow e_3$	–0.542	–0.465	–0.673		–0.323
	–0.407	–0.454	–0.678		0.424
		–0.609	–0.393	0.853	
$b_2 \rightarrow e_3$		–0.593	–0.395	0.782	
		–0.593	–0.399	0.611	
		–0.571	–0.345	–0.763	0.415
$a_1 \rightarrow e_1$		–0.563	–0.347	–0.704	0.407
		–0.553	–0.344	–0.641	0.613
	12605.8	15227.1	16650.3	27715.5	32235.1
ΔE [cm^{-1}]	12636.9	15228.0	16646.2	24652.2	32271.2
	12637.3	15227.4	16645.9	23669.4	32248.1
	0.077	0.0192	0.0657	0.0257	2.46
f	0.051	0.0181	0.0654	0.0223	2.37
	0.005	0.0178	0.0651	0.0146	1.4
	Ex/CR	Ex	Ex	CR	Ex/CR

Table X: INDO/S-CI calculated exited states of neutral Eu $(OEP)_2$. Only the xz polarized CI coefficients are given, for the yz polarized differing in phase. Only those transitions with an oscillator strength f > 0.005 are reported.

State	Dominant conf. CI coeff.	ΔE [cm^{-1}]	f	ΔE_{exp} [a)] [cm^{-1}]	Comments
$^8E_2$	$b_2 \rightarrow a_2$, 0.960	7853	0.000		
$^8E_2$	$a_1 \rightarrow a_2$, 0.967	8508	0.000	7812	NIR,CR
$^8E_2$	$b_1 \rightarrow a_2$, 0.990	9025	0.304		
$^8E_1$	$b_2 \rightarrow e_3$, 0.624 $a_1 \rightarrow e_1$, 0.496	15297	0.0004	14900	Q_{0a}
$^8E_1$	$a_2 \rightarrow e_1$, 0.694 $b_2 \rightarrow e_3$, 0.441 $a_1 \rightarrow e_1$, 0.331	17209	0.019	17200	Q_{0b}
$^8E_1$	$b_2 \rightarrow e_3$, 0.399 $a_1 \rightarrow e_1$, 0.405 $b_1 \rightarrow e_3$, 0.399	18790	0.037	18500	Q_1
$^8E_1$	$b_2 \rightarrow e_3$, 0.577 $b_1 \rightarrow e_3$, 0.700	21340	0.025		
$^8E_1$	$a_1 \rightarrow e_1$, 0.443 $a_1 \rightarrow e_3$, 0.665 $b_2 \rightarrow e_3$, 0.417 $b_1 \rightarrow e_1$, 0.478	23347	0.004	20000	Q'' (broad)
$^8E_1$	$a_1 \rightarrow e_1$, 0.503 $a_1 \rightarrow e_3$, 0.448 $b_2 \rightarrow e_1$, 0.343 $b_1 \rightarrow e_1$, 0.368	23426	0.012	—	$\pi \rightarrow \pi^*$
$^8E_1$	$a_1 \rightarrow e_1$, 0.532 $b_2 \rightarrow e_3$, 0.478 $b_2 \rightarrow e_1$, 0.453 $b_1 \rightarrow e_1$, 0.398	23676	0.006	—	$\pi \rightarrow \pi^*$
$^8E_2$	$a_1 \rightarrow e_1$, 0.551	24085	0.013	—	$\pi \rightarrow \pi^*$
$^8E_2$	$b_2 \rightarrow e_1$, 0.823 $b_2 \rightarrow e_3$, 0.335	29448	0.168	—	$\pi \rightarrow \pi^*$
$^8E_2$	$a_1 \rightarrow e_1$, 0.439 $b_2 \rightarrow e_1$, 0.567	29708	0.248	—	$\pi \rightarrow \pi^*$
$^8E_1$	$a_1 \rightarrow e_1$, 0.693 $b_1 \rightarrow e_3$, 0.421	35350	6.964	26600	B (broad)

a) Ref. 5.

Active

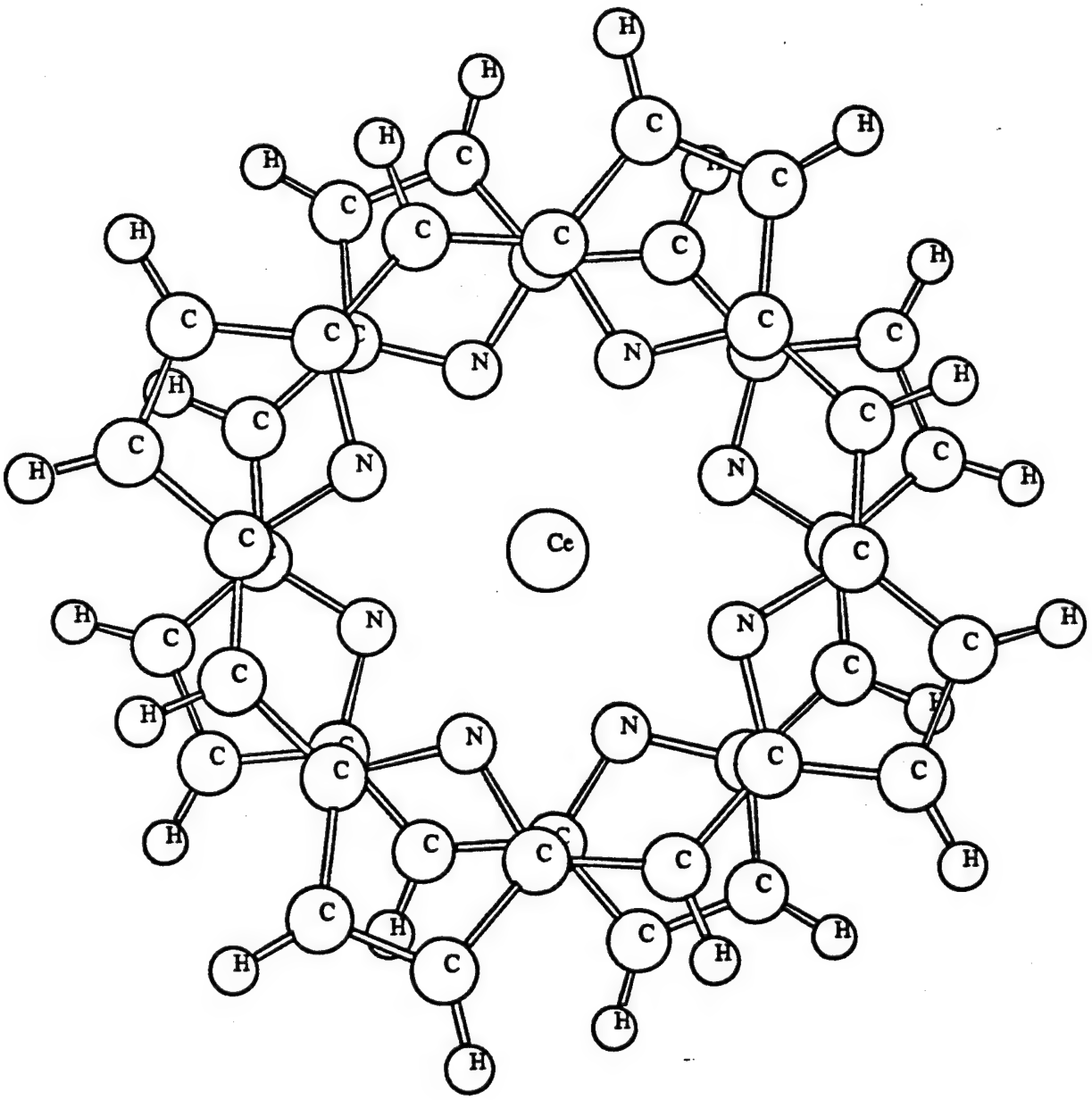

Active

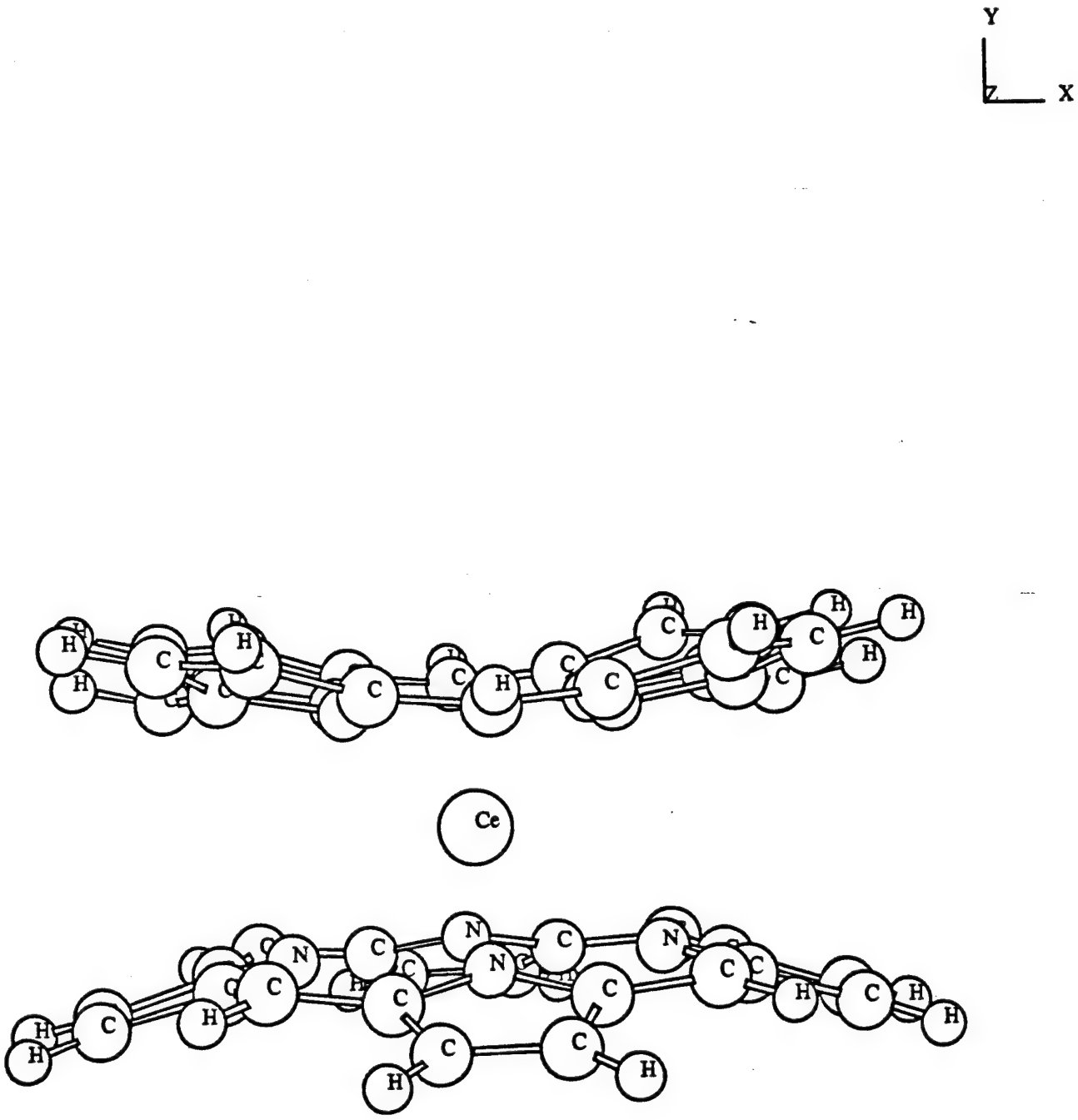

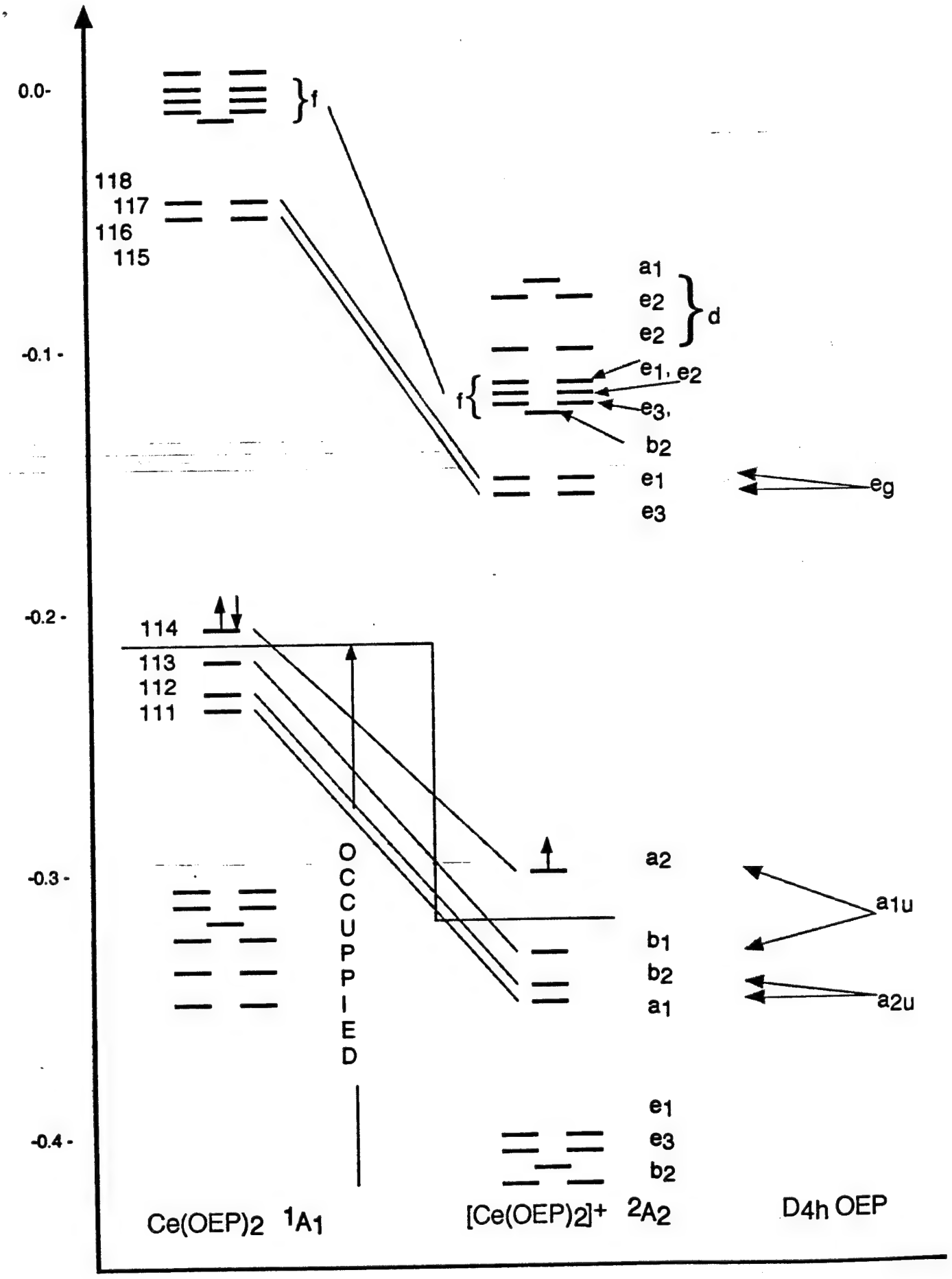
0.0-
-0.1 -
-0.2 -
-0.3 -
-0.4 -
118
117
116
115
f
114
113
112
111
OCCUPPIED
a1
e2
e2
d
f
e1, e2
e3,
b2
e1
e3
eg
a2
b1
b2
a1
a1u
a2u
e1
e3
b2
Ce(OEP)2 1A1
[Ce(OEP)2]+ 2A2
D4h OEP

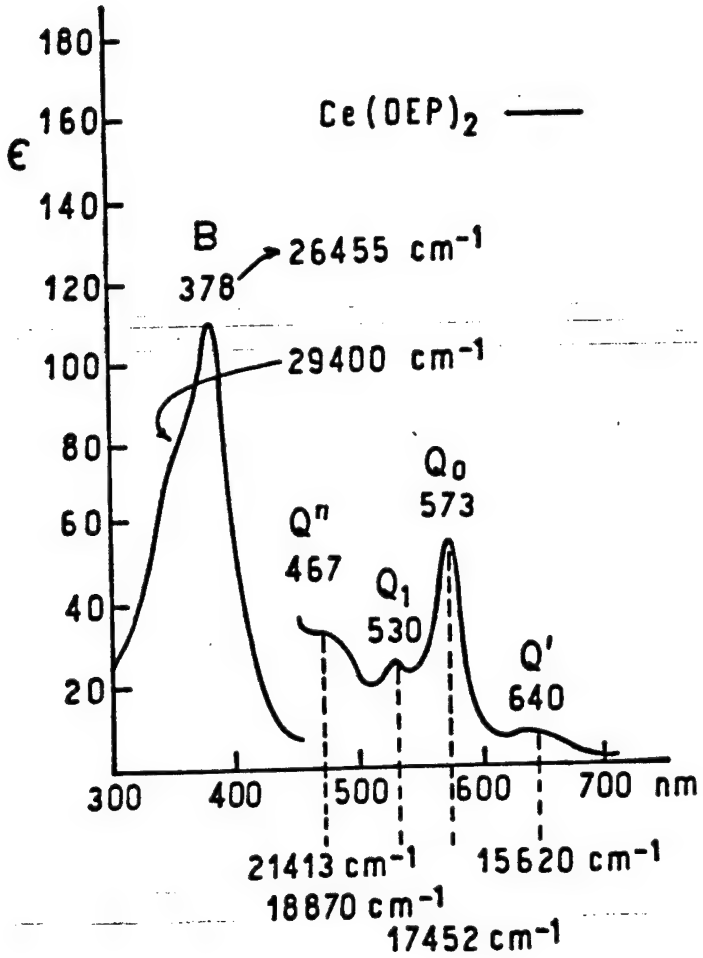
180
160
140
120
100
80
60
40
20
ε
Ce(OEP)2
B
378
26455 cm-1
29400 cm-1
Qn
467
Q1
530
Q0
573
Q'
640
300
400
500
600
700 nm
21413 cm-1
18870 cm-1
17452 cm-1
15620 cm-1

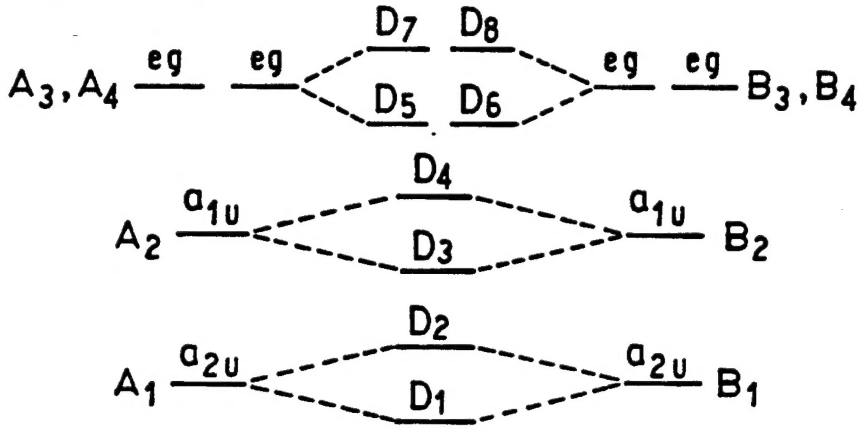
D7
D8
A3, A4
eg
eg
eg
eg
B3, B4
D5
D6
D4
a1u
a1u
A2
B2
D3
D2
a2u
a2u
A1
B1
D1

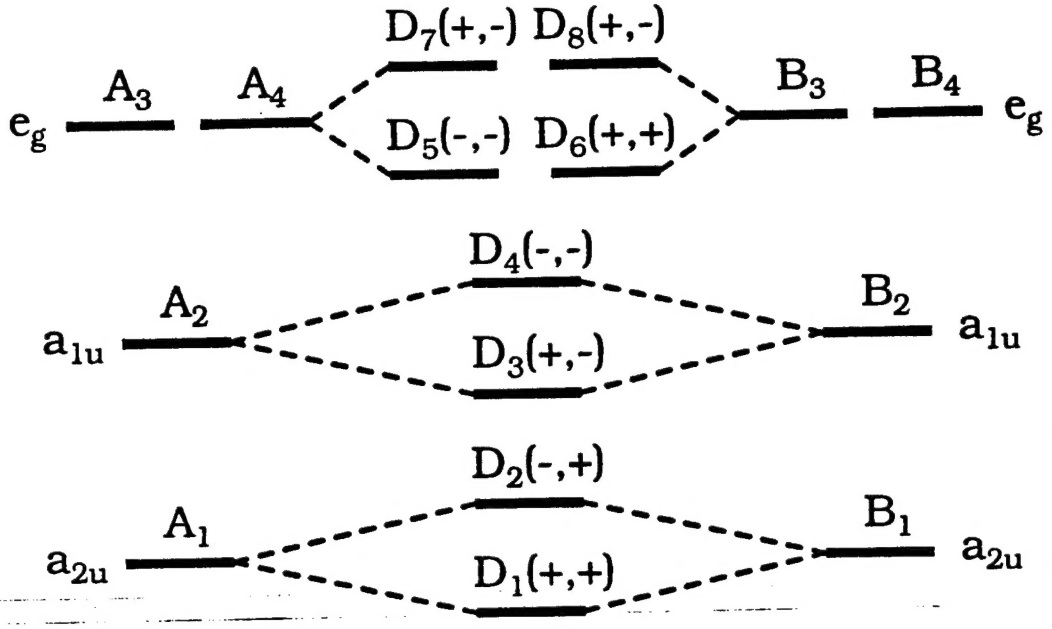
$D_7(+,-)$ $D_8(+,-)$
A_3 A_4 B_3 B_4
e_g e_g
$D_5(-,-)$ $D_6(+,+)$
$D_4(-,-)$
A_2 B_2
a_{1u} a_{1u}
$D_3(+,-)$
$D_2(-,+)$
A_1 B_1
a_{2u} a_{2u}
$D_1(+,+)$

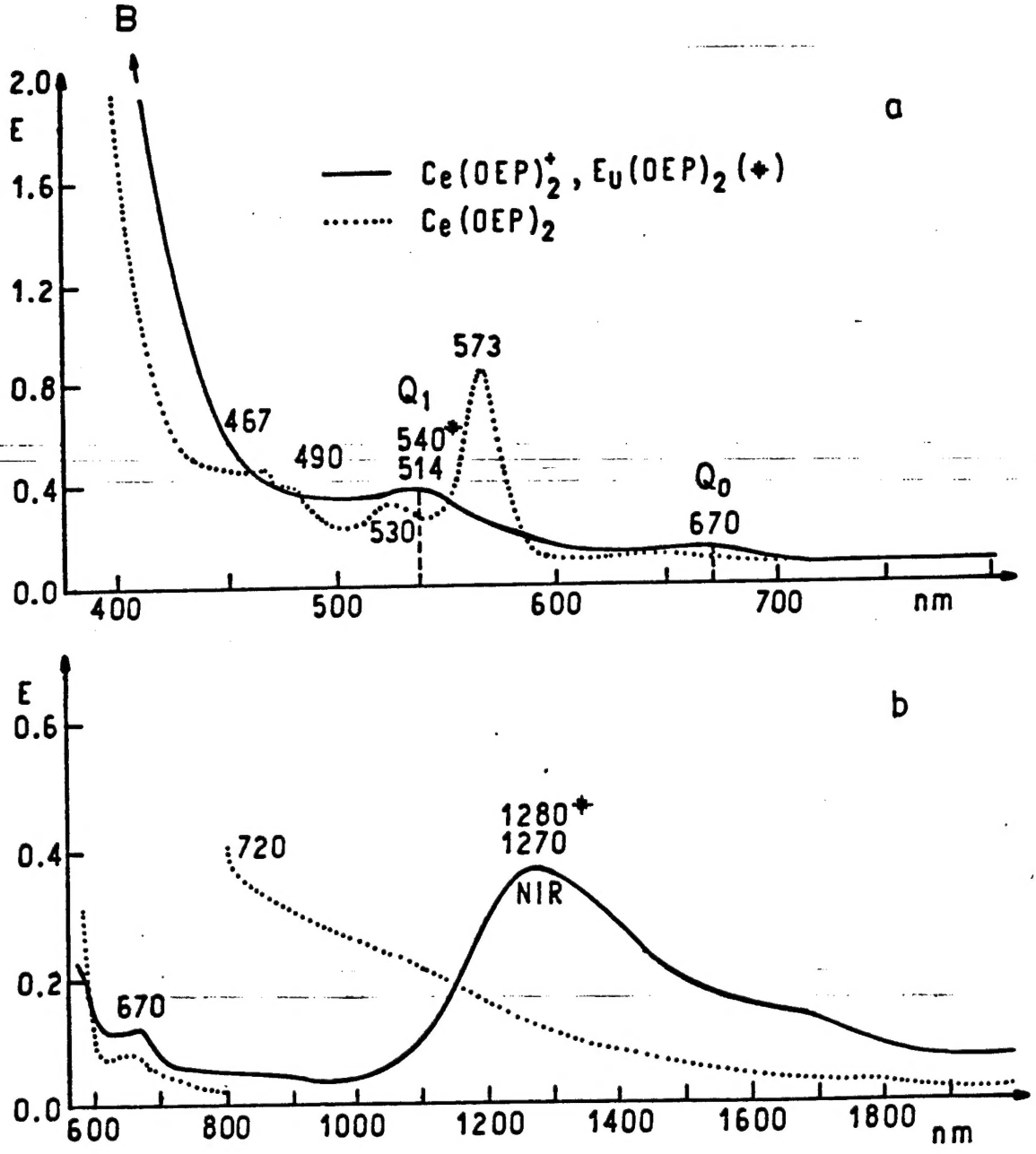
B
2.0
E
1.6
1.2
0.8
0.4
0.0
a
Ce(OEP)$_2^+$, Eu(OEP)$_2$ (+)
Ce(OEP)$_2$
573
Q$_1$
467
490
540+
514
530
Q$_0$
670
400
500
600
700
nm
E
0.6
0.4
0.2
0.0
b
1280+
1270
720
NIR
670
600
800
1000
1200
1400
1600
1800
nm

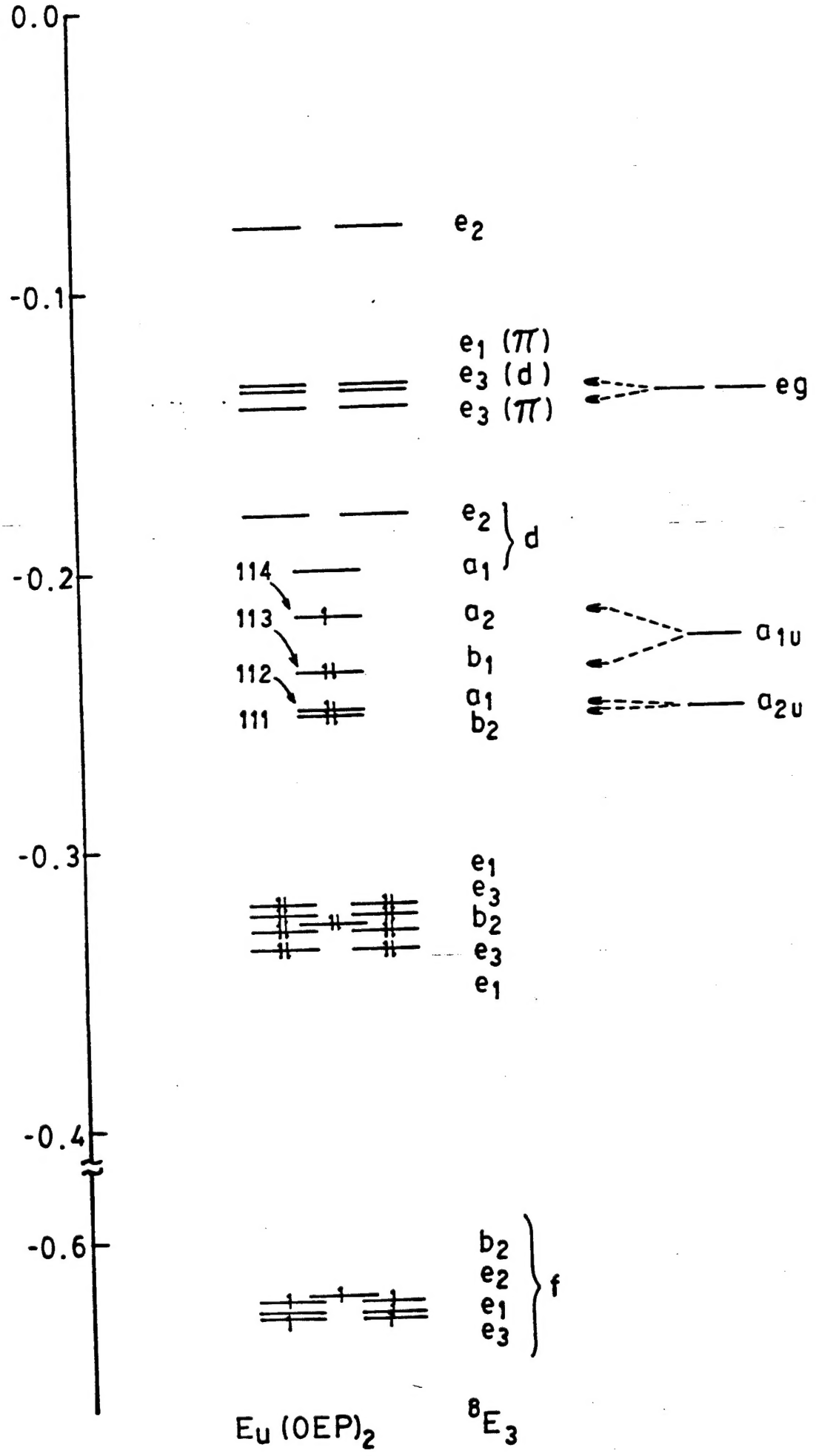
0.0
-0.1
-0.2
-0.3
-0.4
-0.6
e2
e1 (π)
e3 (d)
e3 (π)
eg
e2
a1
d
114
113
112
111
a2
b1
a1
b2
a1u
a2u
e1
e3
b2
e3
e1
b2
e2
e1
e3
f
Eu (OEP)2
8E3